Energy transfer in anisotropic magnetohydrodynamic turbulence

B. Teaca,[1,2] M. K. Verma,[3] B. Knaepen,[1] and D. Carati[1]
[1]*Statistical and Plasma Physics, Université Libre de Bruxelles, Campus Plaine, CP 231, B-1050 Brussels, Belgium*
[2]*Faculty of Physics, University of Craiova, A.I. Cuza 13, 200585 Craiova, Romania*
[3]*Department of Physics, Indian Institute of Technology, 208016 Kanpur, India*
(Received 28 November 2008; revised manuscript received 3 March 2009; published 14 April 2009)

A spectral analysis of anisotropic magnetohydrodynamic turbulence, in presence of a constant magnetic field, is presented using high-resolution direct numerical simulations. A method of decomposing the spectral space into ring structures is presented and the energy transfers between such rings are studied. This decomposition method takes into account the angular dependency of energy transfers in anisotropic systems, while it allows one to recover easily the known shell-to-shell energy transfers in the limit of isotropic turbulence. For large values of the constant magnetic field, the total-energy transfer appears to be most dominant in the direction perpendicular to the mean magnetic field. The linear transfer due to the constant magnetic also appears to be important in redistributing the energy between the velocity and the magnetic fields.

DOI: 10.1103/PhysRevE.79.046312 PACS number(s): 47.65.−d, 47.27.ek, 47.27.er

I. INTRODUCTION

The strong couplings between different scales in a flow represent one of the primary attributes of turbulence. In the turbulent regime, they are expressed mathematically by the nonlinear terms that enter the fluid balance equations and they dominate the dynamics of the flow. In three-dimensional fluid turbulence, these couplings are the channel used to transfer the kinetic energy from the large-scale range to the small-scale range where dissipation takes place. In magnetohydrodynamics (MHD), the momentum balance equation is influenced by the Lorentz force and the number of nonlinear terms is three instead of one of fluid turbulence. Various channels can then be used to transfer the energy from the large scales to the dissipative range.

The energy transfers in both fluid and MHD turbulence are usually presented in spectral space by computing the energy exchanges between the Fourier modes. The energy transfers between modes in turbulence are completely characterized by triad interactions [1]. However, for strong-turbulence regimes, the total number of modes active in the system is too large to be represented systematically by the triad interactions. Since the majority of modes have similar properties as their wave-number neighbors and bring similar contribution to the energy exchange between scales, the analysis of energy transfers is usually simplified by partitioning the spectral space into subdomains and looking at the averaged energy transfers between these subdomains [2]. The partitioning of the spectral domain is arbitrary but several convenient geometrical structures are preferred. The spectral spherical symmetry present in the case of isotropic turbulence naturally suggests a decomposition of the spectral domain into wave-number shells. For this case the energy transfer is described in terms of shell-to-shell transfer functions and spherical energy fluxes that have been studied in detail [3–6].

In the presence of a mean magnetic field, the flow develops a preferred direction and exhibits anisotropy. The degree of anisotropy depends on the strength of the mean magnetic field [7,8]. The angular dependence with respect to the preferred direction then becomes as relevant as the wave-vector amplitude in the spectral space partition, and a simple shell decomposition is not sufficient for getting a more detailed picture of energy transfers. Coaxial cylindrical domains aligned with the preferred direction and planar domains transverse to each direction have both been used in the past to partition the spectral space [9]. In this paper, we propose another partition that is based on a ring decomposition of shells. Similar to the scheme proposed by Alexakis *et al.* [9], the present approach provides many details on the energy transfers in an anisotropic system. This information is very useful for better understanding of the dynamics in anisotropic turbulence that in turn will help in developing large-eddy simulation (LES) models for MHD turbulence. Moreover, the present approach allows us to recover easily the isotropic transfer functions which have been extensively studied in literature.

II. THEORETICAL FRAMEWORK

The MHD equations for a fluid read in the incompressible limit as

$$\frac{\partial u_i}{\partial t} = -u_j \nabla_j u_i + B_j \nabla_j B_i + \nu \nabla^2 u_i + f_i - \nabla_i p, \tag{1}$$

$$\frac{\partial B_i}{\partial t} = -u_j \nabla_j B_i + B_j \nabla_j u_i + \eta \nabla^2 B_i, \tag{2}$$

where $u_i = u_i(\mathbf{x},t)$ is the fluid velocity field, $B_i = B_i(\mathbf{x},t)$ is the magnetic field expressed in Alfvén units, and $p = p(\mathbf{x},t)$ is the total, hydrodynamic+magnetic, pressure field divided by the constant mass density. The magnetic field B_i is the sum of a constant part B_i^0 and a turbulent part b_i induced by the flow. The fluid viscosity ν and the magnetic diffusivity η are taken to be equal, so that the magnetic Prandtl number ($\mathrm{Pr} = \nu/\eta$) is unity. The divergence-free force $f_i = f_i(\mathbf{x},t)$ used in the present work is chosen to be isotropic so that it does not introduce any preferred direction. Equations (1) and (2) are supplemented by the incompressibility condition for the fluid

$(\nabla_j u_j = 0)$ and the divergence-free condition for the magnetic field $(\nabla_j b_j = 0)$. Because of the incompressibility condition, the pressure p can be formally eliminated by solving the Poisson equation $\nabla^2 p = -\nabla_i u_j \nabla_j u_i + \nabla_i b_j \nabla_j b_i$. By convention, summation over repeated indices is assumed.

In order to describe the dynamics of energy transfers in MHD turbulence, Eqs. (1) and (2) are solved in a periodic box using N Fourier modes in each direction. For a given quantity, the physical Q and the spectral $\hat{Q}$ representations are related using the direct and the inverse discrete Fourier transforms:

$$\hat{Q}(\mathbf{k}) = \frac{1}{N^3} \sum_{\mathbf{x}} Q(\mathbf{x}) e^{-ik_j x_j}, \tag{3}$$

$$Q(\mathbf{x}) = \sum_{\mathbf{k}} \hat{Q}(\mathbf{k}) e^{ik_j x_j}. \tag{4}$$

The spectral representations of Eqs. (1) and (2) are easily derived and read:

$$\frac{\partial \hat{u}_i(\mathbf{k})}{\partial t} = -ik_j \sum_{\Delta} \hat{u}_j(\mathbf{q}) \hat{u}_i(\mathbf{p}) + ik_j \sum_{\Delta} \hat{b}_j(\mathbf{q}) \hat{b}_i(\mathbf{p}) + ik_j B_j^0 \hat{b}_i(\mathbf{k}) - \nu k^2 \hat{u}_i(\mathbf{k}) + \hat{f}_i(\mathbf{k}) - ik_i \hat{p}(\mathbf{k}), \tag{5}$$

$$\frac{\partial \hat{b}_i(\mathbf{k})}{\partial t} = -ik_j \sum_{\Delta} \hat{u}_j(\mathbf{q}) \hat{b}_i(\mathbf{p}) + ik_j \sum_{\Delta} \hat{b}_j(\mathbf{q}) \hat{u}_i(\mathbf{p}) + ik_j B_j^0 \hat{u}_i(\mathbf{k}) - \eta k^2 \hat{b}_i(\mathbf{k}), \tag{6}$$

where the notation Σ_Δ stands for the summation over all values of the vectors $\mathbf{p}$ and $\mathbf{q}$ under the constraint that $\mathbf{p}+\mathbf{q}=\mathbf{k}$. The evolution of the kinetic energy $[E^u(\mathbf{k}) = \frac{1}{2}|\hat{\mathbf{u}}(\mathbf{k})|^2]$ and the magnetic energy $[E^b(\mathbf{k}) = \frac{1}{2}|\hat{\mathbf{b}}(\mathbf{k})|^2]$ carried on by the modes with wave vector $\mathbf{k}$ are easily derived from these equations:

$$\frac{\partial E^u(\mathbf{k})}{\partial t} = -\sum_{\Delta} S^u_{u,u}(\mathbf{k}|\mathbf{p}|\mathbf{q}) + \sum_{\Delta} S^u_{b,b}(\mathbf{k}|\mathbf{p}|\mathbf{q}) + L_{ub}(\mathbf{k}) - 2\nu k^2 E^u(\mathbf{k}) + P_f(\mathbf{k}), \tag{7}$$

$$\frac{\partial E^b(\mathbf{k})}{\partial t} = -\sum_{\Delta} S^b_{b,u}(\mathbf{k}|\mathbf{p}|\mathbf{q}) + \sum_{\Delta} S^b_{u,b}(\mathbf{k}|\mathbf{p}|\mathbf{q}) - L_{ub}(\mathbf{k}) - 2\eta k^2 E^b(\mathbf{k}), \tag{8}$$

where

$$P_f(\mathbf{k}) = \mathrm{Re}\{\hat{f}_i(\mathbf{k}) \hat{u}_i^*(\mathbf{k})\}, \tag{9}$$

$$L_{ub}(\mathbf{k}) = k_j B_j^0 \, \mathrm{Im}\{\hat{u}_i(\mathbf{k}) \hat{b}_i^*(\mathbf{k})\}, \tag{10}$$

and where Re and Im represent the real and imaginary parts of a complex number, respectively, and * denotes the complex conjugation. The quantity $S^X_{Y,Z}(\mathbf{k}|\mathbf{p}|\mathbf{q})$ is defined as

$$S^X_{Y,Z}(\mathbf{k}|\mathbf{p}|\mathbf{q}) = \mathrm{Im}\{[k_j \hat{Z}_j(\mathbf{q})][\hat{Y}_i(\mathbf{p}) \hat{X}_i^*(\mathbf{k})]\} \tag{11}$$

and represents the energy transfer from the mode $\mathbf{p}$ of field Y to the mode $\mathbf{k}$ of field X from the interaction with the mode $\mathbf{q}$ of field Z that respects the condition $\mathbf{k}=\mathbf{p}+\mathbf{q}$. Up to a sign, the functions $S^X_{Y,Z}(\mathbf{k}|\mathbf{p}|\mathbf{q})$ represent the *mode-to-mode energy-transfer rate* introduced in [3,10]. The role of $\hat{Z}_j(\mathbf{q})$ is here assumed to be the mediator of the energy exchange. The energy equations contain nonlinear $S^X_{Y,Z}$ and linear L_{ub} transfer terms as well as dissipative terms proportional to ν and η and source terms P_f. The terminologies "nonlinear" and "linear" transfers refer to the nature of the terms in the MHD equations that are responsible for these energy exchanges. Although, strictly speaking, the induction equation only contains one nonlinear term that can be expressed as the curl of the cross product between the velocity and the magnetic field, it is here split into two parts. Both parts have a structure reminiscent from the nonlinear convective and Lorentz force terms in the velocity equation. In terms of energy exchanges, these two terms have quite distinct roles. The first one, $-u_j \nabla_j b_i$, conserves the magnetic energy, while the second term, $b_j \nabla_j u_i$, corresponds to the magnetic energy gain from the exchange with the kinetic energy. This latter term exactly compensates for the loss of kinetic energy due by the Lorentz force. In terms of the energy transfers $S^X_{Y,Z}(\mathbf{k}|\mathbf{p}|\mathbf{q})$, the conservation of the kinetic energy by the convective nonlinearity $-u_j \nabla_j u_i$ is expressed as

$$0 = S^u_{u,u}(\mathbf{k}|\mathbf{p}|\mathbf{q}) + S^u_{u,u}(\mathbf{k}|\mathbf{q}|\mathbf{p}) + S^u_{u,u}(\mathbf{p}|\mathbf{q}|\mathbf{k}) + S^u_{u,u}(\mathbf{p}|\mathbf{k}|\mathbf{q}) + S^u_{u,u}(\mathbf{q}|\mathbf{k}|\mathbf{p}) + S^u_{u,u}(\mathbf{q}|\mathbf{p}|\mathbf{k}), \tag{12}$$

while the conservation of the magnetic energy by the term $-u_j \nabla_j b_i$ is expressed by

$$0 = S^b_{b,u}(\mathbf{k}|\mathbf{p}|\mathbf{q}) + S^b_{b,u}(\mathbf{k}|\mathbf{q}|\mathbf{p}) + S^b_{b,u}(\mathbf{p}|\mathbf{q}|\mathbf{k}) + S^b_{b,u}(\mathbf{p}|\mathbf{k}|\mathbf{q}) + S^b_{b,u}(\mathbf{q}|\mathbf{k}|\mathbf{p}) + S^b_{b,u}(\mathbf{q}|\mathbf{p}|\mathbf{k}). \tag{13}$$

It is important to note that the kinetic and magnetic energies are not conserved individually. The conservation of the total energy by the MHD equations translates into the following rather intricate relation:

$$0 = S^u_{b,b}(\mathbf{k}|\mathbf{p}|\mathbf{q}) + S^u_{b,b}(\mathbf{k}|\mathbf{q}|\mathbf{p}) + S^u_{b,b}(\mathbf{p}|\mathbf{q}|\mathbf{k}) + S^u_{b,b}(\mathbf{p}|\mathbf{k}|\mathbf{q}) + S^u_{b,b}(\mathbf{q}|\mathbf{k}|\mathbf{p}) + S^u_{b,b}(\mathbf{q}|\mathbf{p}|\mathbf{k}) + S^b_{u,b}(\mathbf{k}|\mathbf{p}|\mathbf{q}) + S^b_{u,b}(\mathbf{k}|\mathbf{q}|\mathbf{p}) + S^b_{u,b}(\mathbf{p}|\mathbf{q}|\mathbf{k}) + S^b_{u,b}(\mathbf{p}|\mathbf{k}|\mathbf{q}) + S^b_{u,b}(\mathbf{q}|\mathbf{k}|\mathbf{p}) + S^b_{u,b}(\mathbf{q}|\mathbf{p}|\mathbf{k}), \tag{14}$$

Moreover, the following antisymmetry property is automatically satisfied:

$$S^X_{Y,Z}(\mathbf{k}|\mathbf{p}|\mathbf{q}) = -S^Y_{X,Z}(\mathbf{p}|\mathbf{k}|\mathbf{q}). \tag{15}$$

It simply states that the energy given by the mode $\mathbf{p}$ to the mode $\mathbf{k}$ is opposite to the energy the mode $\mathbf{p}$ receives from mode $\mathbf{k}$, no matter what are the fields to which the modes $\mathbf{k}$ and $\mathbf{p}$ belong to. Finally, it must be noted that the linear transfer terms, in the form given by Eq. (10) representing the energy gained by u from b, cancel themselves exactly for each mode independently.

Statistically stationary state is reached when the turbulence is fully developed. For this state, the energy ε injected by the force $\hat{f}_i$ is equal to the energy losses due to kinetic and magnetic dissipative effects. Moreover, the energy content of the spectral modes is also stationary in this state. However, the fluctuations in the energy balance for a single mode [Eq. (7) and (8)] are very large. Hence for meaningful statistical result we need to average over a Fourier subdomain containing similar modes. Sometimes we also need to employ time averaging. The choice for partitioning the entire Fourier space into disjoint subdomains is motivated by the physical properties of the flow. Each subdomain is indeed expected to represent a set of modes with similar properties. However, at this stage, it is not necessary to give an explicit definition for this partitioning and it will be only assumed to be characterized by two integer indices $\{m,\alpha\}$. The choice of a sharp decomposition of the spectral space (disjoint subdomains) compared to a smooth decomposition (overlapping subdomains) was validated by the studies in [11,12]. The equation for the energy stored in each of the subdomain is thus trivially derived from Eqs. (7) and (8):

$$\frac{\partial}{\partial t}E^{u\{m,\alpha\}} = N_u^{u\{m,\alpha\}} + N_b^{u\{m,\alpha\}} + L_{ub}^{\{m,\alpha\}} - D^{u\{m,\alpha\}} + P^{f\{m,\alpha\}}, \tag{16}$$

$$\frac{\partial}{\partial t}E^{b\{m,\alpha\}} = N_b^{b\{m,\alpha\}} + N_u^{b\{m,\alpha\}} - L_{ub}^{\{m,\alpha\}} - D^{b\{m,\alpha\}}. \tag{17}$$

The energy evolution equations first contain contribution from the nonlinearities in the MHD equations. The terms

$$N_Y^{X\{m,\alpha\}} \equiv \sum_{\{n,\beta\}} T_{Y\{n,\beta\}}^{X\{m,\alpha\}} \tag{18}$$

correspond to the sum of the nonlinear energy transfers $T_{Y\{n,\beta\}}^{X\{m,\alpha\}}$ to the field X in the ring $\{m,\alpha\}$ from the field Y in the ring $\{n,\beta\}$. Each of these nonlinear transfers is itself the sum of a large number of triadic interactions:

$$T_{u\{n,\beta\}}^{u\{m,\alpha\}} = \sum_{\mathbf{k}\in\{m,\alpha\}} \sum_{\mathbf{p}\in\{n,\beta\}} -S_{u,u}^{u}(\mathbf{k}|\mathbf{p}|\mathbf{q}), \tag{19}$$

$$T_{b\{n,\beta\}}^{u\{m,\alpha\}} = \sum_{\mathbf{k}\in\{m,\alpha\}} \sum_{\mathbf{p}\in\{n,\beta\}} +S_{b,b}^{u}(\mathbf{k}|\mathbf{p}|\mathbf{q}), \tag{20}$$

$$T_{b\{n,\beta\}}^{b\{m,\alpha\}} = \sum_{\mathbf{k}\in\{m,\alpha\}} \sum_{\mathbf{p}\in\{n,\beta\}} -S_{b,u}^{b}(\mathbf{k}|\mathbf{p}|\mathbf{q}), \tag{21}$$

$$T_{u\{n,\beta\}}^{b\{m,\alpha\}} = \sum_{\mathbf{k}\in\{m,\alpha\}} \sum_{\mathbf{p}\in\{n,\beta\}} +S_{u,b}^{b}(\mathbf{k}|\mathbf{p}|\mathbf{q}). \tag{22}$$

The major advantage of these definitions is that they naturally satisfy the following expected antisymmetry property:

$$T_{Y\{n,\beta\}}^{X\{m,\alpha\}} = -T_{X\{m,\alpha\}}^{Y\{n,\beta\}}. \tag{23}$$

The other terms in Eqs. (16) and (17) are defined by

$$L_{ub}^{\{m,\alpha\}} = \sum_{\mathbf{k}\in\{m,\alpha\}} L_{ub}(\mathbf{k}), \tag{24}$$

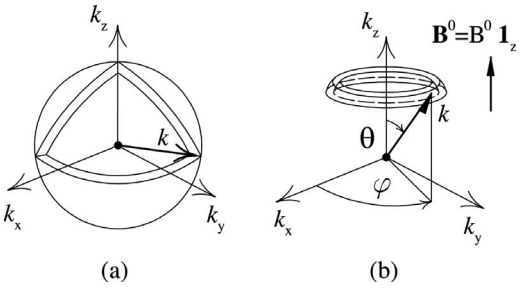

FIG. 1. (a) Shell decomposition; (b) ring decomposition.

$$D^{u\{m,\alpha\}} = 2\nu \sum_{\mathbf{k}\in\{m,\alpha\}} k^2 E^u(\mathbf{k}), \tag{25}$$

$$D^{b\{m,\alpha\}} = 2\eta \sum_{\mathbf{k}\in\{m,\alpha\}} k^2 E^b(\mathbf{k}), \tag{26}$$

$$P^{f\{m,\alpha\}} = \sum_{\mathbf{k}\in\{m,\alpha\}} P_f(\mathbf{k}). \tag{27}$$

In Sec. III, the Fourier-space partitioning is based on a ring decomposition. The first index m in the partition $\{m,\alpha\}$ corresponds to the spherical shell decomposition, commonly used in the investigation of isotropic turbulence. It is based on the division of the spectral space along the wave-vector norm k. A shell s_m contains all the wave vectors $\mathbf{k}$ with the property $k_m \leq |\mathbf{k}| < k_{m+1}$ [Fig. 1(a)]. The set of shell boundaries $\{k_m\}$ may of course depend on the problem. The second index α corresponds to the angular dependency. For simplicity, the mean magnetic field is assumed to be aligned with $\mathbf{1}_z$. The wave vector $\mathbf{k}$ forms an angle θ with respect to the B^0, with $\theta \in [0,\pi]$. The spectral domain is split into angular sections a_α so that each section contains the wave vectors that have the angle θ bounded by $\theta_{\alpha-1} \leq \theta < \theta_\alpha$. The intersection between the spherical shells and the angular sections defines the ring structures $r_{m\alpha} = s_m \cap a_\alpha$ [Fig. 1(b)]. We term the rings near $\theta = \pi/2$ as *equatorial rings*, and the rings near $\theta = 0$ and $\theta = \pi$ as *polar rings*.

In the present paper we will compute energy-transfer functions (19)–(22) from one ring to another. However, the ring-to-ring energy transfers defined by Eqs. (19)–(22) must be normalized in order to compensate for the difference in number of modes in each angular section. For this reason, defining $A_\alpha = [\cos\theta_{\alpha-1} - \cos\theta_\alpha]$, the following quantities are introduced:

$$\bar{T}_{Y\{n,\beta\}}^{X\{m,\alpha\}} = \frac{1}{A_\alpha A_\beta} T_{Y\{n,\beta\}}^{X\{m,\alpha\}}. \tag{28}$$

We term the above energy-transfer function as *ring-to-ring energy-transfer function*. Also, for the same reason, any quantity Q decomposed into ring variables will be normalized accordantly:

$$\bar{Q}^{X\{m,\alpha\}} = \frac{1}{A_\alpha} Q^{X\{m,\alpha\}}. \tag{29}$$

As it can be observed from Fig. 2, the angular normalization ensures that a spherical symmetry is observed for isotropic

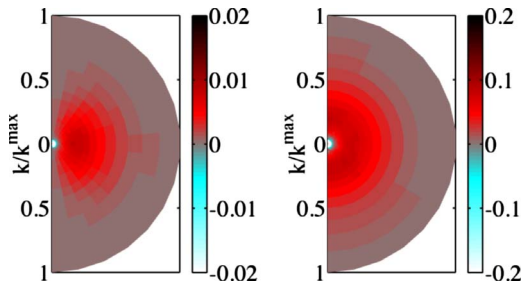

FIG. 2. (Color online) The total nonlinear energy transfers to each ring of field u from field b for the isotropic cases without angular normalization (left) and with angular normalization (right).

turbulence. It must be noted however that, according to previous works on the subject [4–6,12,13], no normalization factor is used for compensating for the number of modes in a shell, roughly proportional to $k_m^2(k_{m+1}-k_m)$. Hence, as long as shell-to-shell transfers are concerned, absolute values will be considered. Energy-transfer functions (28) have the following interesting properties:

(a) Since the normalization factor is symmetric in (α,β), the functions $\bar{T}^{X\{m,\alpha\}}_{Y\{n,\beta\}}$ inherit the antisymmetry property of the non-normalized transfers: $\bar{T}^{X\{m,\alpha\}}_{Y\{n,\beta\}}=-\bar{T}^{Y\{n,\beta\}}_{X\{m,\alpha\}}$.

(b) We can compute the shell-to-shell energy transfers by summing the ring-to-ring energy transfer over the angular sections,

$$T^{X\{m\}}_{Y\{n\}}=\sum_{\alpha}\sum_{\beta}A_\alpha A_\beta \bar{T}^{X\{m,\alpha\}}_{Y\{n,\beta\}}. \tag{30}$$

The ring-to-ring energy-transfer functions have angular dependence for anisotropic situations. However, under isotropic conditions, the energy-transfer function $\bar{T}^{X\{m,\alpha\}}_{Y\{n,\beta\}}$ exhibits several interesting properties listed below:

(a) Since there is no preferred direction in isotropic situations, the net ring-to-ring energy transfer along the polar direction should be zero for a given shell:

$$\bar{T}^{X\{m,\alpha\}}_{Y\{m,\beta\}}=0. \tag{31}$$

(b) The transfer of energy between two given shells depends only on the difference between the angular sections:

$$\bar{T}^{X\{m,\alpha\}}_{Y\{n,\beta\}}=\bar{T}^{X\{m,\alpha+\ell\}}_{Y\{n,\beta+\ell\}}, \tag{32}$$

$$\bar{T}^{X\{m,\alpha\}}_{Y\{n,\alpha+\ell\}}=\bar{T}^{X\{m,\alpha\}}_{Y\{n,\alpha-\ell\}}, \tag{33}$$

where ℓ is an integer.

Note however that the instantaneous ring-to-ring energy transfers are often very noisy, especially at low k because these rings contain only few modes. Therefore we need to perform time averaging to compute the average energy-transfer functions. In addition to the above properties, in the inertial range, the self-similarity implies that

$$\bar{T}^{X\{m,\alpha\}}_{Y\{n,\beta\}}=\bar{T}^{X\{m+a,\alpha\}}_{Y\{n+a,\beta\}}. \tag{34}$$

From the ring-to-ring transfer we can also determine the radial energy flux (coming out of a wave-number sphere)

$$\Pi^{X>}_{Y<}(k_l)=\sum_{n\le l}\sum_{\beta}\sum_{m>l}\sum_{\alpha}T^{X\{m,\alpha\}}_{Y\{n,\beta\}}, \tag{35}$$

and the angular energy flux (coming out of a cone of angle θ_γ)

$$\Pi^{X>}_{Y<}(\theta_\gamma)=\sum_{n}\sum_{\beta\le\gamma}\sum_{m}\sum_{\alpha>\gamma}T^{X\{m,\alpha\}}_{Y\{n,\beta\}}. \tag{36}$$

As mentioned earlier, the expression for the energy transfers between two rings is somewhat arbitrary since these transfers always involve three modes. However, fluxes (35) and (36) are unambiguous because they represent the total energy leaving due to a given nonlinear term.

III. NUMERICAL RESULTS

The MHD equations are solved by a pseudospectral code [14] in a box of length $\mathcal{L}=2\pi$ with periodic boundary conditions with a resolution of $N=512$ modes in each direction. The largest wave number is thus $k^{\max}=256$. The time step is computed automatically by a Courant-Friedricks-Lewey (CFL) criterion and the time advancement is based on a third-order Runge-Kutta scheme. The nonlinear terms are partially dealiased using a phase-shift method [15,16].

The force used in the present work is local in Fourier space. It acts on all the modes within the shell $s_f=[k_{\inf}=2.4, k_{\sup}=3.1]$. With such a choice of the forcing shell boundaries, the number of forced modes is $N_f=104$. The forcing injects in each of the forced mode a constant rate of energy $\varepsilon_e(\mathbf{k})=\varepsilon/N_f$ and a constant rate of helicity $\varepsilon_h(\mathbf{k})=h/N_f$. The large number of forced modes ensures that no anisotropy effect is induced by the forcing mechanism. The total energy and helicity injection rates are thus ε and h, respectively, and represent the forcing control parameters along with the forcing shell s_f. In practice, the force $\hat{\mathbf{f}}$ has the form

$$\hat{\mathbf{f}}(\mathbf{k})=\alpha(\mathbf{k})\hat{\mathbf{u}}(\mathbf{k})+\beta(\mathbf{k})\hat{\omega}(\mathbf{k}) \tag{37}$$

if $|\mathbf{k}|\in s_f$ and zero otherwise. The vector $\hat{\omega}(\mathbf{k})$ represents the Fourier modes of the vorticity $(\omega=\nabla\times u)$. Defining the helicity as $H(\mathbf{k})=\mathrm{Re}\{\hat{\mathbf{u}}(\mathbf{k})\cdot\hat{\omega}(\mathbf{k})^*\}$, we obtain the real parameters $\alpha(\mathbf{k})$ and $\beta(\mathbf{k})$ as

$$\alpha(\mathbf{k})=\frac{1}{2N_f}\frac{4k^2E^u(\mathbf{k})\varepsilon_e(\mathbf{k})-H(\mathbf{k})\varepsilon_h(\mathbf{k})}{4k^2E^u(\mathbf{k})^2-H(\mathbf{k})^2},$$

$$\beta(\mathbf{k})=\frac{1}{N_f}\frac{H(\mathbf{k})\varepsilon_e(\mathbf{k})-E^u(\mathbf{k})\varepsilon_h(\mathbf{k})}{4k^2E^u(\mathbf{k})^2-H(\mathbf{k})^2}. \tag{38}$$

For the statistical steady state, when the total dissipation (kinetic+magnetic) equals the energy injection rate ε, the Taylor microscale Reynolds number reaches $R_\lambda\approx 210$, and the product between the Kolmogorov length $l_\nu=(\nu^3/\varepsilon)^{1/4}$ and the largest wave number is about $k_{\max}l_\nu\approx 1.23$. In the present study, no helicity is injected by the forcing process.

A first computation has been performed without external magnetic field $(B^0=0)$, which will be referred to as the isotropic run. Once the statistically stationary state is reached,

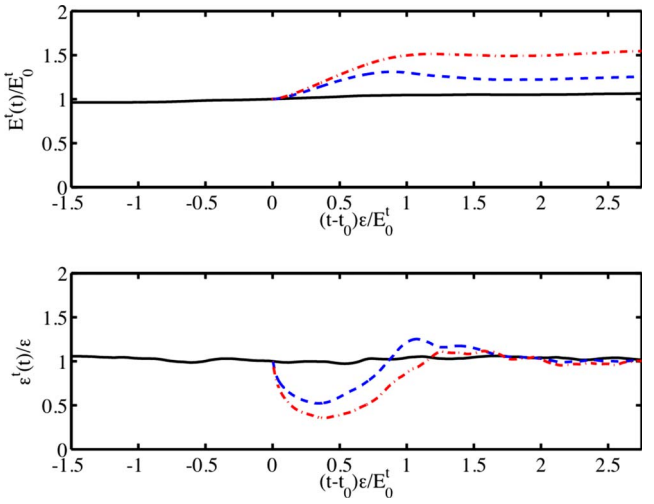

FIG. 3. (Color online) Total-energy (E^t) and total-dissipation (ε^t) evolutions in time. The time at which the external magnetic was switched on is denoted by t_0 and the quantities at that time have the subscript 0. The isotropic case is represented by the solid black line, the weak anisotropic case is denoted by the dashed blue line, and the strong anisotropic case is denoted by the dot-dashed red line.

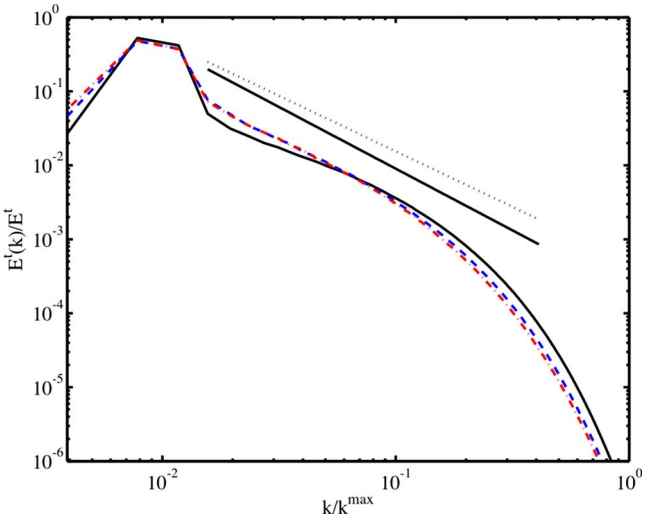

FIG. 4. (Color online) Total-energy [$E^t(k)$] spectra. The isotropic case is represented by the solid black line, the weak anisotropic case is denoted by the dashed blue line, and the strong anisotropic case is denoted by the dot-dashed red line. The dotted line segment has a $-3/2$ slope, while the solid straight line segment has a $-5/3$ slope, and both are shown for reference.

the fluctuations of the magnetic field in isotropic turbulence are measured using the following quantity:

$$\delta b^{\mathrm{iso}} = \sqrt{\frac{1}{\mathcal{L}^3}\int d^3\mathbf{x}\mathbf{b}(\mathbf{x},t)\cdot\mathbf{b}(\mathbf{x},t)}. \tag{39}$$

An ambient magnetic field is then turned on. Two nonzero B^0 that have been considered are $|B^0|=\delta b^{\mathrm{iso}}$ and $|B^0|=\sqrt{10}\delta b^{\mathrm{iso}}$. These two computations will be referred to as the *weak anisotropic* run and the *strong anisotropic* run, respectively. For all runs, the largest one-dimensional integral length scale has been verified to be smaller than the computational box length $\mathcal{L}$.

The time evolution of the total energy ($E^t=E^u+E^b$) and total dissipation ($\varepsilon^t=\varepsilon^u+\varepsilon^b$) for the three cases analyzed below are presented in Fig. 3. The time at which the ambient magnetic field is switched on is denoted by t_0. Using E_0^t (the total energy at time t_0) and the energy injection rate, we define a characteristic time scale $t^*=E_0^t/\varepsilon$. The following ring-transfer diagnostics is performed after the initial transient has disappeared, around $t/t^*=2$. A time average over an interval of $0.5t^*$ has been used to smooth out the statistics when presenting energy transfers and energy fluxes. For the isotropic case the ratio E^u/E^b is about 3.7, while for the weak anisotropic case the value drops to 2.1 For the strong anisotropic case, due to the strong Alfvénization of the energy, the E^u/E^b ratio fluctuates between 1.9 and 2.5. From the expression of the cross helicity,

$$H^c = \frac{1}{\mathcal{L}^3}\int d^3\mathbf{x}\ \mathbf{u}(\mathbf{x},t)\cdot\mathbf{b}(\mathbf{x},t), \tag{40}$$

we determine the cross-helicity coefficient as $H^c/2E^t$. At the time the ring statistics was performed, we had a cross-helicity coefficient of less than 0.01 for the isotropic case, approximately 0.07 for the weak anisotropic case, and a value of 0.03 for the strong anisotropic case.

The spectra $E^t(k)$, $E^t(k_\perp)$, and $E^t(k_\parallel)$, defined as

$$E^t(k_\perp) = 2\pi\int E^t(k)k_\perp dk_\parallel, \tag{41}$$

$$E^t(k_\parallel) = 2\pi\int E^t(k)k_\perp dk_\perp, \tag{42}$$

where $k_\perp=(\mathbf{k}_x^2+\mathbf{k}_y^2)^{1/2}$ and $k_\parallel=|\mathbf{k}_z|$, are shown in Figs. 4 and 5. In order to display smooth spectra, the number of shells used to build the curves in Figs. 4 and 5 is typically $N/2=256$. It is much larger than the number of shells used in the discussion of shell-to-shell energy transfers. In our anisotropic simulations, the anisotropic spectrum in the perpendicular direction seems to indicate a $k_\perp^{-3/2}$ inertial range power law. This is in agreement with other works that have

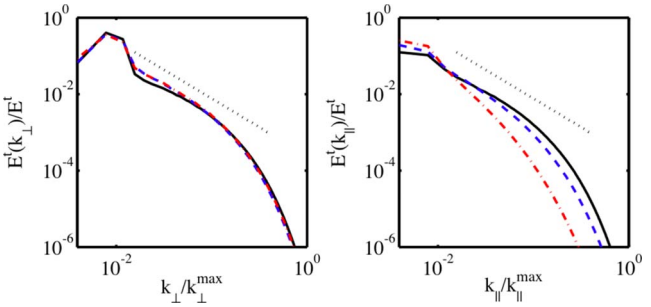

FIG. 5. (Color online) Total-energy (E^t) spectra. The isotropic case is represented by the solid black line, the weak anisotropic case is denoted by the dashed blue line, and the strong anisotropic case is denoted by the dot-dashed red line. The dotted line segment has a $-3/2$ slope.

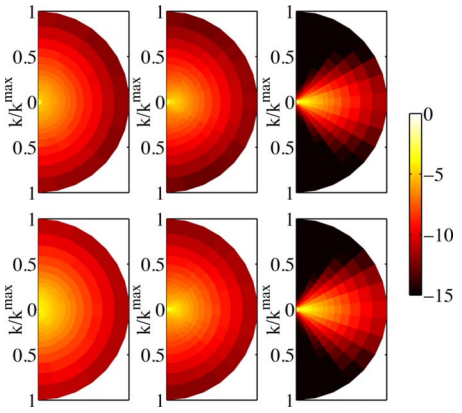

FIG. 6. (Color online) Ring representations of the logarithms ($\log_{10}$) of the kinetic (top) and of the magnetic (bottom) energies. Left to right columns indicate the isotropic, weak anisotropic, and strong anisotropic runs. The values are normalized to the total energy.

studied this aspect in detail [17,18]. Also, the spectrum in the $k_{\parallel}$ direction becomes steeper with the increase in B^0 value [9]. For the isotropic spectra, the choice for the inertial range power-law exponent is not obvious.

The analysis of the energy transfers is based on a partition of the Fourier space using $N_s=23$ spherical shells and 15 angular sections. The shells are defined by $s_n=[k_n,k_{n+1}]$, in which k_n is given by the law $k_n=2^{(n+8)/4}$. The first three shells are however defined differently, $s_1=[0,2]$, $s_2=[2,4]$, and $s_3=[4,8]$, in order to ensure that these shells contain enough modes. The angular sections are taken as constant, with an angular separation of 12°. The eighth angular section is centered on the equatorial plane. The energy injection rate ε due to the forcing is split equally between the 104 modes contained in the wave-number shell $2.4 \leq k < 3.1$. Hence, the forcing is isotropic and acts only in the shell s_2. The force is identical for the three runs. In Figs. 2 and 6–10, the three-dimensional Fourier space is projected on a plane in which the shells s_n are represented by annuli with a width proportional to $k_{n+1}-k_n$. The plane is further split into the angular sections a_α. The intersections of the annuli and the angular sections represent the projections of the rings into a plane and the intensities of the variables in these rings are color (grayscale) coded. Only half of the plane is represented since each ring has two symmetric intersections with it. As a first example of this representation, the kinetic and magnetic energies are shown in Fig. 6. Clearly, the energy levels do not exhibit a strong angular dependence in the weakly anisotropic run.

Throughout the paper, all the figures related to the terms that appear in Eqs. (16) and (17) use the same color range. The values displayed are normalized to the total dissipation ε. The plots take into account the width of each shell for which the boundaries have been normalized to the largest wave number $k^{\max}$.

Dissipation levels are represented in Fig. 7. For all three cases, the total magnetic dissipation is about twice the total kinetic dissipation. Since the total dissipation has to be equal to the energy injection rate, the respective levels of kinetic and magnetic dissipations are thus almost the same in the

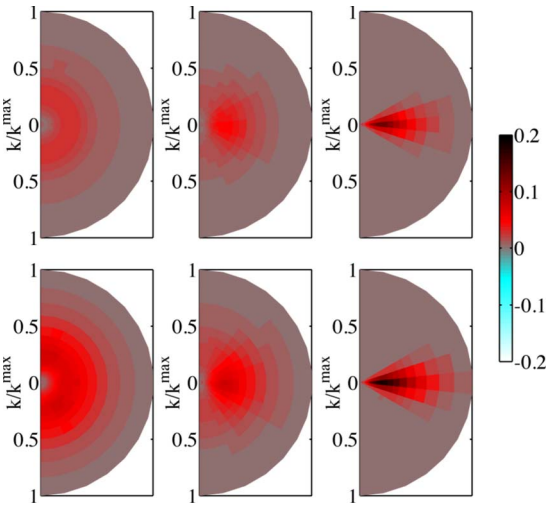

FIG. 7. (Color online) Ring representations of the kinetic (top) and magnetic (bottom) dissipations. Left to right columns indicate the isotropic, weak anisotropic, and strong anisotropic runs.

three runs. In the isotropic run, no angular variation is observed up to slight fluctuations. On the contrary, in the anisotropic runs, the levels of dissipation are clearly angle dependent. The dissipation in the direction of B^0 tends to be suppressed, and the suppression increases with the increase in the imposed magnetic field. Since global kinetic and magnetic dissipations are about the same as in the isotropic case, the decrease in dissipation in the direction parallel to the constant magnetic field has to be compensated for by an increase in dissipation in the perpendicular direction. This behavior is stronger for larger degrees of anisotropy.

The linear energy exchange rate $\bar{L}_{ub}^{\{m,\alpha\}}$ is shown in Fig. 8 using a similar representation. Of course, because this term is proportional to $\mathbf{k}\cdot\mathbf{B}^0$, it is only presented for the two anisotropic runs and it has to vanish in the direction perpendicular to $\mathbf{B}^0$. Interestingly, the transfer is also suppressed in the parallel direction for larger degrees of anisotropy and tends to concentrate toward the *equatorial rings* with the increase in the ambient magnetic field value.

The complete description of ring-to-ring energy transfers $\bar{T}_{Y\{m,\beta\}}^{X\{m,\alpha\}}$ would require a four-dimensional representation or a large number of two-dimensional figures. Instead of a long collection of figures, we first present the total energy transferred to a ring from all the other rings ($\bar{N}_Y^{X\{m,\alpha\}}$) in Fig. 9. The angular dependency of the transfer functions is evident.

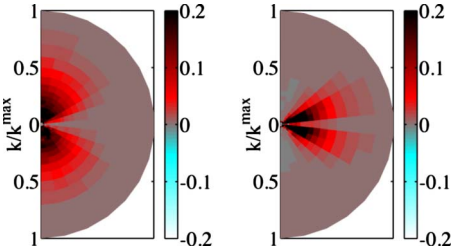

FIG. 8. (Color online) Ring representations of the linear transfers $\bar{L}_{ub}^{\{m,\alpha\}}$ for weak anisotropy (left) and strong anisotropy (right).

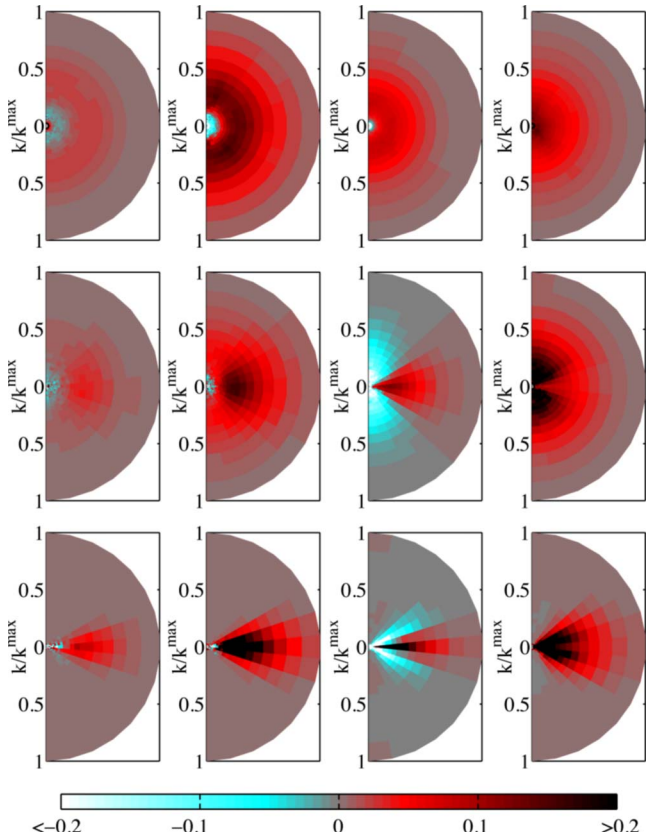

FIG. 9. (Color online) The total nonlinear energy transfer to each ring. Left to right columns indicate $\bar{N}_u^{u\{m,\alpha\}}$, $\bar{N}_b^{b\{m,\alpha\}}$, $\bar{N}_b^{u\{m,\alpha\}}$, and $\bar{N}_u^{b\{m,\alpha\}}$. Top to bottom represent the isotropic, weak anisotropic, and strong anisotropic runs.

It is interesting to observe that the cross-field transfer (between the velocity and the magnetic fields) changes sign depending on the direction to B^0 for the anisotropic cases. With the increase in B^0, the rings near the equator have stronger energy transfer compared to the ones near the poles.

These features can be largely explained by the global phenomenology of energy transfers. Indeed, the energy is injected into the system in kinetic form only and in the forcing range which is very close to the smallest shells. It is dissipated in the large wave-number shells, both by viscous and Joule effects. Since the analysis is performed in a statistically stationary regime, energy has to flow from u to b and from small to large shells. Also, outside the forcing range, the dissipation in a shell has to be exactly balanced by the total nonlinear transfer to this shell. Indeed, when summing the energy transferred to u and b, the linear transfers cancel exactly. Hence, the dissipation (Fig. 7) in a shell is also the total-energy transfer to this shell, and it is clear that in the anisotropic cases, energy is preferentially transferred toward the equatorial plane.

The local energy transfer is among the same u and b modes. Under steady state, the energy transfer is from u to b fields to rings both above and below the equator, but close to the equator. Hence, the energy transfer due to linear term is also concentrated near the equator. As we will show later, the energy accumulated due to the linear term is distributed to

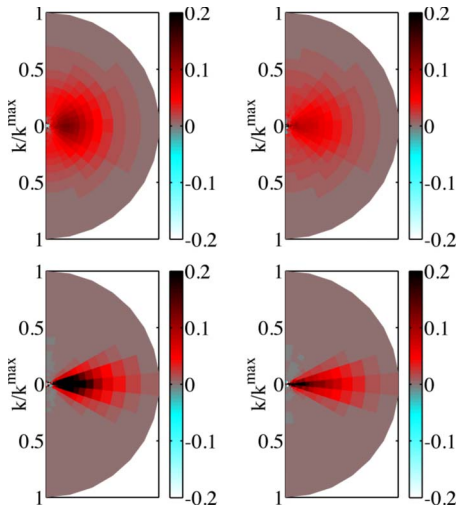

FIG. 10. (Color online) The total cross-field energy transfer to each ring, left column for $\bar{N}_b^{u\{m,\alpha\}}+\bar{L}_{ub}^{\{m,\alpha\}}$ and right column for $\bar{N}_u^{b\{m,\alpha\}}-\bar{L}_{ub}^{\{m,\alpha\}}$, for weak anisotropy (top) and strong anisotropy (bottom), respectively.

the other modes near equator due to nonlinear interactions.

Finally, due to the linear term, energy is constantly and locally, i.e. inside the same shell, redistributed between u and b. Combining these effects largely explains Fig. 9, in which one can see that kinetic energy is pumped from large scales and from the poles and is locally redistributed by linear effects to the magnetic field and redistributed through nonlinear transfers to the equatorial plane in both kinetic and magnetic forms. In the strong anisotropic case, almost no energy is left close to the poles and the absolute transfers from the pole region are very small.

Obviously, the linear and nonlinear contributions to the cross-field transfer have quite different patterns. In Fig. 10, both contributions are added to get the total transfer between u and b. This total transfer tends to be more and more localized in the perpendicular direction to the mean magnetic field when B^0 increases. Moreover, it is significantly smoother than both the linear and the nonlinear transfers, indicating that the anisotropic linear transfer is partially compensated by the nonlinear transfers. Hence, although the nonlinear transfers do not explicitly depend on the ambient magnetic field, they become anisotropic because they redistribute kinetic and magnetic energies that have been affected by the presence of $\mathbf{B}^0$ in the linear terms.

A more detailed picture of the energy exchange can be obtained from the analysis of the ring-to-ring transfer functions. In the following, this analysis is limited to shells 8–11 that correspond to the interval $k=[16,32]$. Although the resolution is relatively too low to observe a well-developed inertial range, this interval of wave vectors does exhibit a sort of plateau in the energy transfer. The giver shell is fixed to $n=9$ and the receiving shell m varies in the above-mentioned interval. The transfer between angular sections is then analyzed. Figure 11 presents the case of isotropic turbulence. It is observed that the overall energy transfer from shell n to shell $m=8$ is negative, while the transfer to shell $m=10$ is positive. This confirms the direct energy cascade of energy

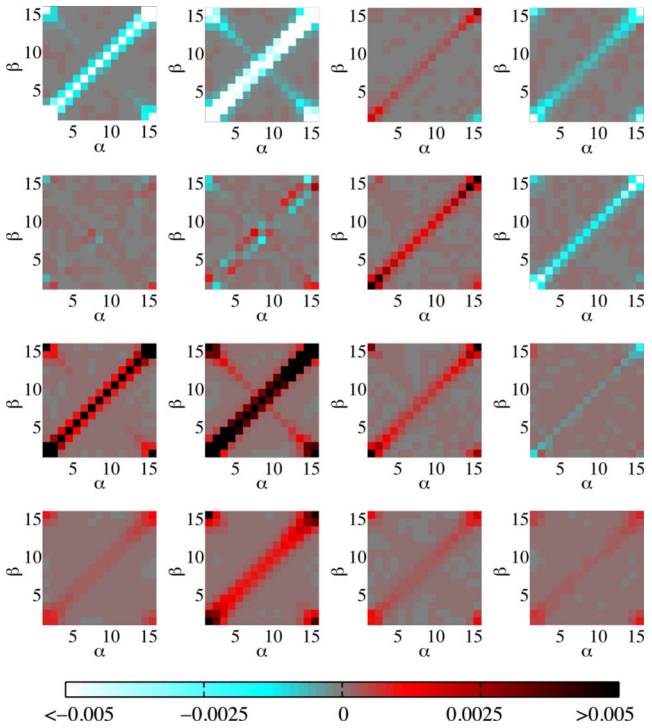

FIG. 11. (Color online) Energy transfers between angular sections for given shells (isotropic case). Left to right columns indicate $\bar{T}^{u\{m,\alpha\}}_{u\{n,\beta\}}$, $\bar{T}^{b\{m,\alpha\}}_{b\{n,\beta\}}$, $\bar{T}^{u\{m,\alpha\}}_{b\{n,\beta\}}$, and $\bar{T}^{b\{m,\alpha\}}_{u\{n,\beta\}}$. For all cases $n=9$ (the giver shell index) and from top to bottom, $m=8$, $m=9$, $m=10$, and $m=11$ (the receiver shell indices).

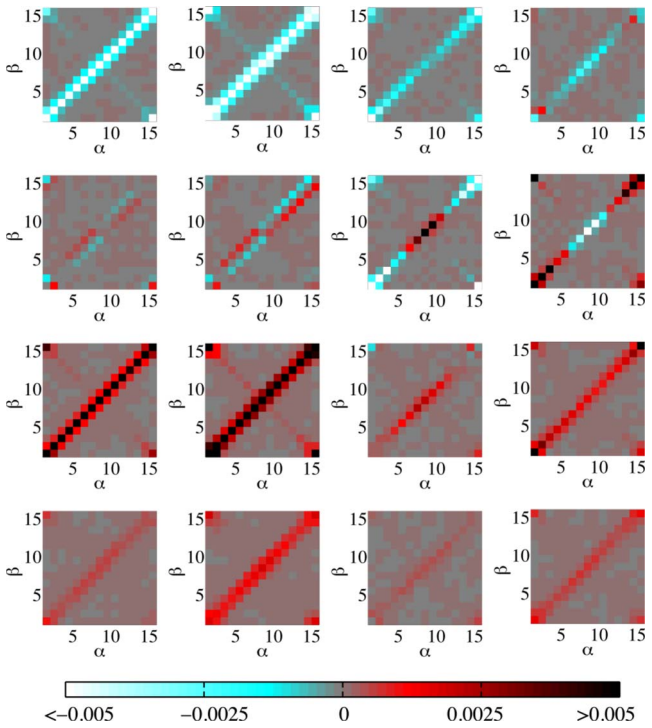

FIG. 12. (Color online) Energy transfers between angular sections for given shells (weak anisotropic case). Left to right columns indicate $\bar{T}^{u\{m,\alpha\}}_{u\{n,\beta\}}$, $\bar{T}^{b\{m,\alpha\}}_{b\{n,\beta\}}$, $\bar{T}^{u\{m,\alpha\}}_{b\{n,\beta\}}$, and $\bar{T}^{b\{m,\alpha\}}_{u\{n,\beta\}}$. For all cases $n=9$ (the giver shell index) and from top to bottom, $m=8$, $m=9$, $m=10$, and $m=11$ (the receiver shell indices).

(kinetic and magnetic) since the transfer from a shell corresponding to a large scale to a shell corresponding to a small scale is positive. Also, on average, for $n=m$, the u-to-u and b-to-b energy transfers are zero, as imposed by formula (31). Although some transfers are not strictly zero, they remain very small and simply correspond to fluctuation that would disappear if a lengthy time averaging was performed. Moreover, the sum over the angular sections vanishes exactly. The locality of the shell energy transfer is also observed since for shell $m=11$ the transfer is very much reduced. From shell-to-shell analysis, it is known that the cross-field transfer is strongest inside the same shell. The transfer between angular sections representation shows that it is also local in angular sections as the strongest contribution is observed for $\alpha=\beta$.

The same quantities from the anisotropic runs are shown in Figs. 12 and 13. The same features are observed concerning the locality of interactions and the direct cascades. However, the angular dependence becomes more pronounced for higher B^0. For the strong anisotropic case, the dominant energy transfer takes place among the rings that are perpendicular to the mean magnetic field (near the equator). There is hardly any energy transfer among the rings near the poles. The following properties are observed for the ring-to-ring energy transfer under anisotropic situations:

(a) The ring-to-ring energy transfers $\bar{T}^{u\{m,\alpha\}}_{u\{n,\beta\}}$, $\bar{T}^{b\{m,\alpha\}}_{b\{n,\beta\}}$, $\bar{T}^{u\{m,\alpha\}}_{b\{n,\beta\}}$, and $\bar{T}^{b\{m,\alpha\}}_{u\{n,\beta\}}$ are local and forward when $m \neq n$. Careful observations of Figs. 12 and 13 show that the energy transfers from shell n to $n+1$ shell are toward the equator.

(b) When $m=n$ (same shell), the ring-to-ring energy transfer is essentially local; that is, energy flows dominantly from angular section $\alpha \pm 1$ to α. Also, $\bar{T}^{u\{n,\alpha\}}_{u\{n,\alpha+1\}} > 0$ and $\bar{T}^{b\{n,\alpha\}}_{b\{n,\alpha+1\}} > 0$ for $\alpha=1-7$, but $\bar{T}^{u\{n,\alpha\}}_{u\{n,\alpha+1\}} < 0$ and $\bar{T}^{b\{n,\alpha\}}_{b\{n,\alpha+1\}} < 0$ for $\alpha=9-15$. This implies that the u-to-u and b-to-b energies flow toward the poles (direction parallel to the mean magnetic field) within a given shell. Among all T, $\bar{T}^{u\{n,7\}}_{u\{n,8\}}$, $\bar{T}^{b\{n,7\}}_{b\{n,8\}}$, $\bar{T}^{u\{n,8\}}_{u\{n,9\}}$, and $\bar{T}^{b\{n,8\}}_{b\{n,9\}}$ are the most dominant. In summary, there is significant u-to-u and b-to-b energy transfers among the rings in the same shell, and the energy transfers are strongest near the equator.

(c) For b-to-u transfer, there is a strong energy transfer from a b ring to the u ring of the same ring index. For the ring at the equator, $\bar{T}^{u\{m,8\}}_{b\{n,8\}} > 0$. The b-to-u energy transfers for the other rings however have opposite signs, i.e., $\bar{T}^{u\{m,\alpha\}}_{b\{n,\alpha\}} < 0$ around $\alpha \neq 8$. By definition the u-to-b energy transfer is exactly opposite to the b-to-u energy transfer. These results are consistent with the energy transfers shown in Fig. 9, where the *equatorial rings* of u receive energy from b field, while, the nonequatorial rings give energy to the b field.

IV. CONCLUSIONS

The energy transfer in anisotropic MHD turbulence has been studied using a ring decomposition of the spectral space. The source of anisotropy is the external ambient magnetic field $\mathbf{B}^0$. Three runs have been compared. One run corresponds to the isotropic system ($\mathbf{B}^0=0$), and the other two

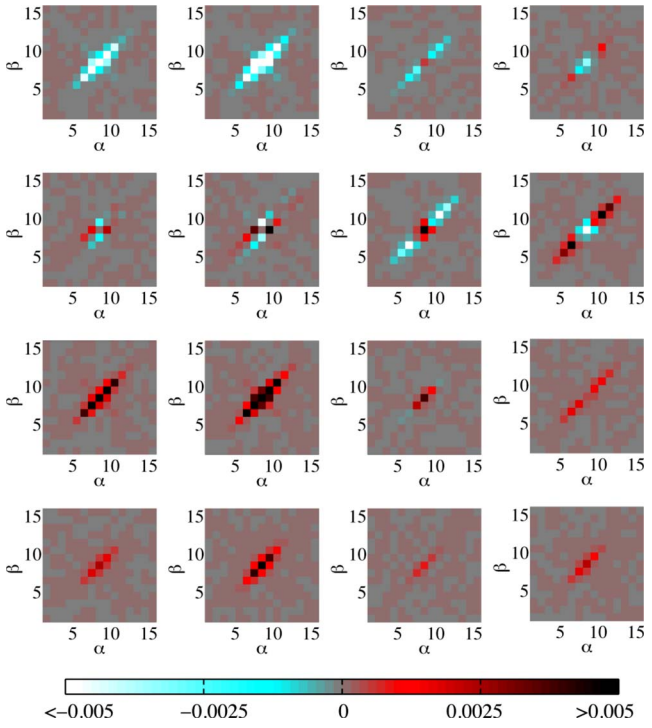

FIG. 13. (Color online) Energy transfers between angular sections for given shells (strong anisotropic case). Left to right columns indicate $\bar{T}^{u\{m,\alpha\}}_{u\{n,\beta\}}$, $\bar{T}^{b\{m,\alpha\}}_{b\{n,\beta\}}$, $\bar{T}^{u\{m,\alpha\}}_{b\{n,\beta\}}$, and $\bar{T}^{b\{m,\alpha\}}_{u\{n,\beta\}}$. For all cases $n=9$ (the giver shell index) and from top to bottom: $m=8$, $m=9$, $m=10$, and $m=11$ (the receiver shell indices).

cases are nonzero $\mathbf{B}^0$ that have been referred to as the weakly anisotropic and strongly anisotropic runs. The energy, energy dissipation, and energy transfers in the presence of a constant magnetic field have been shown to depend on the angular section. The anisotropy becomes more pronounced when the strength of the mean magnetic field is increased.

We analyze the energy transfers among various rings in the spectral space. We observe that the dominant energy transfer is in the direction perpendicular to the mean magnetic field, and the energy transfers parallel to the mean magnetic field are suppressed. These results are in agreement with the results reported in the past. Our detailed study shows that the energy transfers among the rings are also local and forward, i.e., the dominant energy transfer is to the nearest rings, and the direction is from smaller wave-number rings to larger wave-number rings.

For the anisotropic cases, we also find energy transfer within a shell itself. The u-to-u and b-to-b energy transfers tend to be away from the equator. However, transfers between different shells are preferentially directed toward the equator, and globally this later effect dominates the dynamics. The u fields of rings at the equator receive energy from the b field of the same rings. However, the u field of the nonequatorial rings give energy to the b field of the corresponding rings due to nonlinearity.

We also observe significant energy transfer due to the linear term that is proportional to the mean magnetic field; this energy transfer is strongly anisotropic. This is an important feature that might have consequence in MHD turbulence modeling. For instance, there is a reasonable chance that models used in LES of isotropic turbulence would be also suitable for anisotropic MHD turbulence. Indeed, on one side, the information lost when removing the smallest scales in a LES does not affect the linear terms but only the nonlinear terms through mode-to-mode couplings. Anisotropy effects generated by the linear terms would be perfectly captured in an LES. On the other side, the ambient field explicitly affects the linear transfer terms but not the nonlinear terms. The nonlinear transfers only become anisotropic because they redistribute kinetic and magnetic energies that have been affected by the presence of $\mathbf{B}^0$ in the linear terms. There is thus no clear reason to design new models for anisotropic MHD turbulence. The same conclusion was reached in the low-magnetic-Reynolds-number limit [19].

A nonlocal transfer of energy between the forced velocity shell and the small-scale magnetic field has been observed in previous works on forced isotropic turbulence [6,13]. These nonlocal interactions are clearly related to the forcing and only affect the forced velocity shell which transfers energy to the magnetic field at almost all scales. For the anisotropic cases studied here, these effects are still present and, although not shown here, can be observed in the shell-to-shell transfer functions. However, the ring-to-ring analysis has been performed here for shells located in the inertial range. In this case, the nonlocal effects were not present or they were too weak to be noticed.

Several extensions of this work could be considered. First, a different angular decomposition with more sections close to the equatorial plane might be better adapted to strongly anisotropic runs since the only active exchanges are in this region. However, in that case, the number of mode in these rings might become quite low and a time averaging would become unavoidable in order to reduce the fluctuation level. In the present study, the refinement of the angular decomposition has not been explored since it is not expected to reveal any new phenomenon. Also, the extension of the ring decomposition method for the Elsässer variables is straightforward. Finally, forcing with a nonzero helicity injection rate could also be considered. Preliminary results have already been obtained for such forcing and a change in the partition of energy between the velocity and the magnetic fields is observed, while the total-energy level remains unchanged. A direct consequence of this observation is a change in the intensity of the energy transfers between the velocity and the magnetic field depending on the helicity injection level. The ring decomposition method can also be used to address other aspects, like passive scalar transport and inertial-range scaling laws for anisotropic turbulence [20–28].

ACKNOWLEDGMENTS

The authors would like to acknowledge Paolo Burattini and Maxim Kinet for useful discussions. M.K.V. thanks the Physique Statistique et Plasmas group at the University Libre de Bruxelles for the kind hospitality and financial support during his long leave when this work was undertaken. This

work was sponsored in part by funds from the participating organizations of the EURYI (European Young Investigator) scheme and the EC Sixth Framework Programme. Financial support from the Communauté Française de Belgique (Grant No. ARC 02/07-283) and from the contract of association EURATOM–Belgian state is also gratefully acknowledged. D.C. was supported by the Fonds National pour la Recherche Scientifique (FNRS)–Belgium.

[1] M. Lesieur, *Turbulence in Fluids* (Kluwer Academic, Dordrecht, 1997).
[2] J. A. Domaradzki and R. S. Rogallo, Phys. Fluids A **2**, 413 (1990).
[3] G. Dar, M. K. Verma, and V. Eswaran, Physica D **157**, 207 (2001).
[4] O. Debliquy, M. K. Verma, and D. Carati, Phys. Plasmas **12**, 042309 (2005).
[5] A. Alexakis, P. D. Mininni, and A. Pouquet, Phys. Rev. E **72**, 046301 (2005).
[6] P. D. Mininni, A. Alexakis, and A. Pouquet, Phys. Rev. E **72**, 046302 (2005).
[7] J. V. Shebalin, W. H. Matthaeus, and D. Montgomery, J. Plasma Phys. **29**, 525 (1983).
[8] S. Oughton, E. R. Priest, and W. H. Matthaeus, J. Fluid Mech. **280**, 95 (1994).
[9] A. Alexakis, B. Bigot, H. Politano, and S. Galtier, Phys. Rev. E **76**, 056313 (2007).
[10] M. K. Verma, Phys. Rep. **401**, 229 (2004).
[11] J. A. Domaradzki and D. Carati, Phys. Fluids **19**, 085112 (2007).
[12] J. A. Domaradzki and D. Carati, Phys. Fluids **19**, 085111 (2007).
[13] D. Carati, O. Debliquy, B. Knaepen, B. Teaca, and M. K. Verma, J. Turbul. **7**, 1 (2006).
[14] D. Carati and TURBO team, Solver for TURbulent flows with periodic BOundary conditions, http://www.ulb.ac.be/sciences/spp, 2008.
[15] R. S. Rogallo, NASA Technical Memorandum No. 81315, 1981 (unpublished).
[16] G. S. Patterson and S. A. Orszag, Phys. Fluids **14**, 2538 (1971).
[17] J. Maron and P. Goldreich, Astrophys. J. **554**, 1175 (2001).
[18] J. Mason, F. Cattaneo, and S. Boldyrev, Phys. Rev. E **77**, 036403 (2008).
[19] B. Knaepen and P. Moin, Phys. Fluids **16**, 1255 (2004).
[20] P. Burattini, M. Kinet, D. Carati, and B. Knaepen, Phys. Fluids **20**, 065110 (2008).
[21] P. Burattini, M. Kinet, D. Carati, and B. Knaepen, Physica D **237**, 2062 (2008).
[22] M. Kinet, P. Burattini, D. Carati, and B. Knaepen, Phys. Fluids **20**, 075105 (2008).
[23] R. Kraichnan, J. Fluid Mech. **47**, 525 (1971).
[24] A. Potherat and T. Alboussiere, Phys. Fluids **15**, 3170 (2003).
[25] W. H. Matthaeus, S. Ghosh, S. Oughton, and D. A. Roberts, J. Geophys. Res. **101**, 7619 (1996).
[26] O. Schilling and Y. Zhou, J. Plasma Phys. **68**, 389 (2002).
[27] L. Biferale, E. Calzavarini, A. S. Lanotte, F. Toschi, and R. Tripiccione, Physica A **338**, 194 (2004).
[28] J. Cho and E. T. Vishniac, Astrophys. J. **539**, 273 (2000).